Check for updates

View Article Online
View Journal

Journal of Materials Chemistry A

Accepted Manuscript

This article can be cited before page numbers have been issued, to do this please use: L. Guan, X. Yin, D. Zhao, C. Wang, Q. An, J. Yu, N. Shrestha, C. Grice, R. Awni, Y. Yu, Z. Song, J. Zhou, W. Meng, F. Zhang, R. Ellingson, J. Wang, W. Tang and Y. Yan, *J. Mater. Chem. A*, 2017, DOI: 10.1039/C7TA08053K.

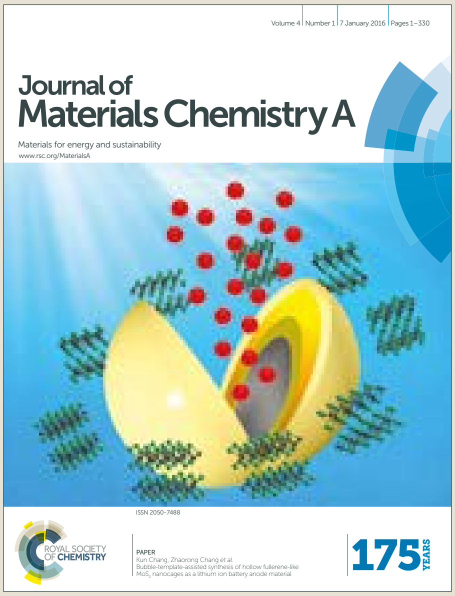

Volume 4 | Number 1 | 7 January 2016 | Pages 1–330

Journal of Materials Chemistry A

Materials for energy and sustainability

www.rsc.org/MaterialsA

ISSN 2050-7488

ROYAL SOCIETY OF CHEMISTRY

PAPER
Kun Chang, Zhaorong Chang et al.
Bubble-template-assisted synthesis of hollow fullerene-like MoS_2 nanocages as a lithium-ion battery anode material

175 YEARS

This is an Accepted Manuscript, which has been through the Royal Society of Chemistry peer review process and has been accepted for publication.

Accepted Manuscripts are published online shortly after acceptance, before technical editing, formatting and proof reading. Using this free service, authors can make their results available to the community, in citable form, before we publish the edited article. We will replace this Accepted Manuscript with the edited and formatted Advance Article as soon as it is available.

You can find more information about Accepted Manuscripts in the author guidelines.

Please note that technical editing may introduce minor changes to the text and/or graphics, which may alter content. The journal's standard Terms & Conditions and the ethical guidelines, outlined in our author and reviewer resource centre, still apply. In no event shall the Royal Society of Chemistry be held responsible for any errors or omissions in this Accepted Manuscript or any consequences arising from the use of any information it contains.

ROYAL SOCIETY OF CHEMISTRY

rsc.li/materials-a

View Article Online
DOI: 10.1039/C7TA08053K

Cost-Effective Hole Transporting Material for Stable and Efficient Perovskite Solar Cells with Fill Factors up to 82%

Lei Guan,[§,a,b] Xinxing Yin,[§,c] Dewei Zhao,[§,b] Changlei Wang,[b] Qiaoshi An,[d] Jiangsheng Yu,[c] Niraj Shrestha,[b] Corey R. Grice,[b] Rasha A. Awni,[b] Yue Yu,[b] Zhaoning Song,[b] Jie Zhou,[c] Weiwei Meng,[b] Fujun Zhang,[d] Randy J. Ellingson,[b] Jianbo Wang,[*,a,e] Weihua Tang,[*,c] and Yanfa Yan[*,b]

[a]School of Physics and Technology, Center for Electron Microscopy, MOE Key Laboratory of Artificial Micro- and Nano-structures, and Institute for Advanced Studies, Wuhan University, Wuhan 430072, China
[b]Department of Physics and Astronomy, Wright Center for Photovoltaics Innovation and Commercialization, The University of Toledo, Toledo, OH 43606, United States.
[c]Key Laboratory of Soft Chemistry and Functional Materials, Nanjing University of Science and Technology, Nanjing 210094, China
[d]Key Laboratory of Luminescence and Optical Information, Beijing Jiaotong University, Beijing 100044, China
[e]Science and Technology of High Strength Structural Materials Laboratory, Central South University, Changsha 410083, China

[§] These authors contributed equally to this work.

***Corresponding authors:**
Jianbo Wang (wang@whu.edu.cn),
Weihua Tang (whtang@njust.edu.cn),
Yanfa Yan (yanfa.yan@utoledo.edu).

View Article Online
DOI: 10.1039/C7TA08053K

Abstract:

A new small molecule-based hole selective material (HSM), 4,4',4''-(7,7',7''-(5,5,10,10,15,15-hexahexyl-10,15-dihydro-5*H*-diindeno[1,2-*a*:1',2'-*c*]fluorene-2,7,12-triyl)tris(2,3-dihydrothieno[3,4-*b*][1,4]dioxine-7,5-diyl))tris(*N,N*-bis(4-methoxyphenyl)aniline) (TRUX-E-T), has been developed by a facile synthesis with reduced cost. The highest occupied molecular orbital energy level and lowest unoccupied molecular orbital energy level of TRUX-E-T are -5.10 and -2.50 eV, respectively, making it a suitable HSM for lead iodide perovskite solar cells. TRUX-E-T can be smoothly deposited onto perovskite layers, enabling efficient perovskite solar cells with thin TRUX-E-T layers (~50 nm), which helps cut the unit cost of the HSL used in PVSCs to approximately one-fortieth (1/40) of 2,2′,7,7′-Tetrakis (*N,N*-di-p-methoxyphenylamino)-9,9′-spirobifluorene (spiro-OMeTAD). Additionally, TRUX-E-T exhibits hole mobility as high as 2.47×10^{-4} cm^2/Vs, better than spiro-OMeTAD. As a result, our perovskite solar cells using TRUX-E-T have shown high fill factors up to 82%. The champion cell achieved a maximum power conversion efficiency of 18.35% (16.44%) when measured under reverse (forward) voltage scan under AM1.5 G 100 mW/cm^2 illumination. Our un-encapsulated cells exhibited good stability in ambient air, maintaining 96.4% of their initial efficiency of 18.35% after 20 days storage.

View Article Online
DOI: 10.1039/C7TA08053K

1. Introduction

Perovskite solar cells (PVSCs) have attracted enormous attention in recent years due to their high optical absorption coefficients and very long carrier lifetimes.[1-6] The power conversion efficiency (PCE) has increased from 3.8% to over 22% in the past few years.[7-16] PVSCs are typically fabricated by sandwiching a perovskite absorber layer with an electron selective layer (ESL) and a hole selective layer (HSL). The ESL and HSL separate and extract photogenerated electrons and holes in the perovskite absorber, respectively. Therefore, the PCE of a PVSC relies significantly on the optoelectronic properties of ESL and HSL materials, such as the energy levels of band edges, bandgaps, and carrier mobility. Inappropriate ESLs and HSLs can adversely affect the open-circuit voltages (V_{oc}s) and fill factors (FFs) of PVSCs.[17, 18] So far, PVSCs with record PCEs typically use TiO_2 ESLs and spiro-OMeTAD is 2,2′,7,7′-Tetrakis (*N,N*-di-p-methoxyphenylamino)-9,9′-spirobifluorene (spiro-OMeTAD) HSLs.[7, 19] The main drawbacks of using spiro-OMeTAD HSLs in PVSCs include: (1) high cost for synthesizing pure spiro-OMeTAD; (2) poor charge transport mobility; (3) requirements for p-type dopants such as cobalt complexes which may result in chemical degradation;[20] (4) low thermal stability and crystallization at temperatures as low as 60 ^{o}C. These drawbacks limit the large-scale commercialization of PVSCs using spiro-OMeTAD HSLs. Compared with polymer semiconductors, organic small-molecule HSLs have some unique advantages, such as easy modification and purification, low-cost solution processing at low temperature, well-defined chemical structures, and molecular weights with negligible batch-to-batch variation.[21-24] For example, triazatruxene is one of such organic small-molecule HSL materials and has been successfully used as HTLs for PVSCs.[25, 26] However, the synthesis of triazatruxene involves harsh phosphorus oxychloride regent that greatly hinders its large-scale application.[25, 26]

Aiming to obtain an ideal HSL with low cost, high thermal stability and high hole transport without using Co dopant, we have designed a new HSL, 4,4',4''-(7,7',7''-(5,5,10,10,15,15-hexahexyl-10,15-dihydro-5*H*-diindeno[1,2-*a*:1',2'-*c*]fluorene-2,7,12-triyl)tris(2,3-dihydrothieno[3,4-*b*][1,4]dioxine-7,5-diyl))tris(*N,N*-bis(4-methoxyphenyl)aniline) (TRUX-E-T), with a planar molecular geometry containing truxene as the core, with

View Article Online
DOI: 10.1039/C7TA08053K

3,4-ethylenedioxythiophene (EDOT) as a π-linker, and methoxy-substituted triphenylamine (TPA) as arms. Unlike the orthogonal spiro core, truxene has a planar and fused molecular structure, which enables the HSL to show strong π-π stacking through intermolecular interactions, thereby leading to enhanced hole mobility. The fully conjugated truxene core also provides great potential for improved thermal and optical stability. Moreover, it offers good chemical versatility to tune solubility, 3D configuration and optoelectronic properties.[27, 28] Compared to triazatruxene, truxene can be synthesized by facile methods and it consists six hydrophobic hexyl chains which should work better for both preventing the perovskite surface from the moisture and suppressing crystal growth of HSL to obtain better film.[27, 29] As proven in previous reports, the incorporation of EDOT unit can enhance charge transport and improve device performance without sacrificing stability.[30, 31] TPA has 3D π-conjugated molecular configuration, which can restrict aggregation and promote exciton separation. The propeller-like structure of TPA is also beneficial for forming uniform and smooth thin films with stable amorphous morphology and homogeneous features.[32] A combination of EDOT bridge with TPA arms can endow TRUX-E-T with suitable energy levels and efficient hole-transporting properties.[18, 25, 26, 33-35]

With the aforementioned considerations, we herein report on the synthesis and characterization of TRUX-E-T and its application as HSLs in efficient PVSCs. We show that high-quality TRUX-E-T can be synthesized by a facile route, ensuring a low cost. Characterizations reveal that the highest occupied molecular orbital (HOMO) and lowest unoccupied molecular orbital (LOMO) energy levels of TRUX-E-T are at -5.10 and -2.50 eV, respectively, which are suitable as HSLs for effective charge transfer in PVSCs. TRUX-E-T exhibits hole mobility as high as 2.47×10^{-4} cm^2/Vs as well as efficient charge transfer at the perovskite/TRUX-E-T interface. As a result, our PVSCs using TRUX-E-T have shown high fill factors (FFs) up to 82%. Additionally, TRUX-E-T can be smoothly deposited on perovskite layers, enabling PVSC to use thin TRUX-E-T layers. Our best-performing PVSCs use only ~50 nm-thick TRUX-E-T HSLs, which helps to reduce the unit cost of the HSL used in PVSCs to approximately one-fortieth (1/40) of that for devices made using spiro-OMeTAD. The champion cell achieved a maximum PCE of 18.35% (16.44%) when measured under revese (forward) voltage scan under AM1.5 G 100 mW/cm^2 illumination.

Our un-encapsulated cell exhibited good stability in ambient air, maintaining 96.4% of its initial efficiency of 18.35% after 20 days storage. It is worth noting that TRUX-E-T HSLs do not require Co complex doping, eliminating a significant route for possible degradation.

2. Experimental section

2.1. Material synthesis

TRUX-E-T: A solution of the compound 2,7,12-tribromo-5,5,10,10,15,15-hexahexyl-10,15-dihydro-5*H*-diindeno[1,2-*a*:1',2'-*c*]fluorene (450.0 mg, 0.42 mmol) and 4-methoxy-*N*-(4-methoxyphenyl)-*N*-(4-(7-(tributylstannyl)-2,3-dihydrothieno[3,4-*b*][1,4]dioxin-5-yl)phenyl)aniline (1.1 g, 1.49 mmol) in dry toluene (40 mL) was degassed twice with N_2, then $Pd(PPh_3)_4$ (71.9 mg, 0.062 mmol) was added. After stirring at 110°C for 48 h under N_2, the mixture was cooled to room temperature. After removal of toluene, the crude product was purified by column chromatography on silica gel (petroleum ether/ethyl acetate, 7:1, v/v) and recrystallized from methanol to afford TRUX-E-T (610.0 mg, 67.5%) as a light-yellow solid. ^1H NMR (500 MHz, $CDCl_3$, δ): 8.34 (d, *J* = 8.5 Hz, 3H), 7.85 (d, *J* = 8.1 Hz, 3H), 7.76 (s, 3H), 7.66 – 7.58 (m, 6H), 7.09 (d, *J* = 8.4 Hz, 12H), 6.96 (d, *J* = 8.0 Hz, 6H), 6.89 – 6.79 (m, 12H), 4.50 – 4.34 (m, 12H), 3.81 (s, 18H), 2.93 (m, 6H), 2.18 – 2.06 (m, 6H), 1.03 – 0.78 (m, 36H), 0.68 – 0.50 (m, 30H). ^{13}C NMR (125 MHz, $CDCl_3$, δ)156.25, 154.56, 147.68, 141.25, 139.16, 139.06, 138.12, 127.21, 126.88, 125.11, 124.26, 121.18, 119.65, 115.09, 65.14, 65.00, 56.10, 55.90, 37.52, 31.95, 29.98, 24.43 , 22.73, 22.67, 14.42, 14.32. MALDI-TOF MS: m/z=2177.0612 $[M+H]^+$, calcd. for $C_{141}H_{153}N_3O_{12}S_3$: 2176.0616.

2.2. Solution preparation

Perovskite precursor: The $MA_{0.7}FA_{0.3}PbI_3$ perovskite precursor was prepared using a mixture of methylammonium iodide (MAI, Dyesol), formamidium iodide (FAI, Dyesol), lead iodide (PbI_2, Alfa Aesar,99.9985%) and lead thiocyanate ($Pb(SCN)_2$, Sigma-Aldrich, 99.5%) in dimethyl sulfoxide (DMSO, Sigma-Aldrich) and *N,N*-dimethylformamide (DMF, Sigma-Aldrich). The details about the precursor preparation can be found in our previous papers.[34, 36-38] The precursor solution was stirred on a hotplate at 60°C for several hours. The

View Article Online
DOI: 10.1039/C7TA08053K

resulted precursor was purified using a 0.45 μm filter before spin-coating

C_{60}-SAM: C_{60}-self-assembly (SAM) (1-Materials) was used as purchased. C_{60}-SAM has a concentration of 4 mg/mL inchlorobenzene (Sigma-Aldrich, 99.8%).

Spiro-OMeTAD: 2,2',7,7'-Tetrakis(*N,N*'-di-p-methoxyphenylamine)-9,9'-spirobifluorene (spiro-OMeTAD) was used to fabricate the reference HSLs and deposited on the perovskite film at 2000 rpm for 60 s. The spiro-OMeTAD was co-doped using Co(II)-bis-(trifluoromethanesulfonyl) imide (TFSI) and Li-TFSI. The spiro-OMeTAD solution was prepared by dissolving 72.3 mg spiro-OMeTAD (Shenzhen Feiming Science and Technology Co., Ltd.) in 1 mL chlorobenzene (CB) with 28 μL 4-tert-butylpyridine (*t*BP) (Sigma-Aldrich), 18 μL Li-TFSI (Sigma-Aldrich) (520 mg/mL in acetonitrile) and 18 μL Co(II)-TFSI salt (FK102, Dyesol) (300 mg/mL in acetonitrile).

TRUX-E-T: A solution of TRUX-E-T/chlorobenzene (20mg/ml) with an additive of 15 μl Li-TFSI (170 mg/mL in acetonitrile) and 8μL *t*BP.

2.3. Device fabrication

The Florine-doped Tin Oxide (FTO) glass substrates were cleaned by ultra-sonication in diluted Micro-90 detergent, deionized water, acetone, and 2-propanol for 15 min, respectively. SnO_2 ETLs were deposited on FTO using a plasma-enhanced atomic layer deposition (PEALD) method[34, 37-42] and then annealed on a hotplate at 100°C for 1 hour in ambient air (approximately 25 °C and 55% relative humidity). The substrates were then transferred into a nitrogen filled glove box. The C_{60}-SAM solution was spin-coated onto the SnO_2 layer at 3000 rpm for 1 min. The perovskite layer was deposited by dripping diethyl ether via the anti-solvent technique. The perovskite film was annealed at 100 ^{o}C for 5 min. Spiro-OMeTAD was deposited on the perovskite film at 3000 rpm for 60 s. The TRUX-E-T was spin-coated on the perovskite film at 3500 rpm for 45s, leading to an approximately 50 nm-thick layer. A layer of 50 nm gold was finally deposited on the top of the HSLs using thermal evaporation. The active area of the device was 0.08 cm^2 as defined by a shadow mask during the Au evaporation. For hole-only devices, a 30 nm PEDOT:PSS layer was coated on ITO substrate, followed by the deposition of TRUX-E-T or spiro-OMeTAD layer and then 8 nm MoO_3, and 75 nm Ag layers. MoO_3 and Ag were thermally evaporated to complete the

View Article Online
DOI: 10.1039/C7TA08053K

device fabrication.

2.4. Film and device characterization

Cross-sectional scanning electron microscopy (SEM) image of the completed devices was taken with Hitachi S-4800. Tapping-mode atomic force microscopy (AFM) images were taken with a Veeco Nanoscope V instrument. Layer thicknesses were determined using a Dektak surface profiler and cross-sectional SEM images. Samples were illuminated through the glass side for photoluminescence (PL) measurements. A 532 nm cw laser at 38 mW cm^{-2} was used as a source of excitation for steady-state PL while a 532 nm pulsed laser (pulse width ~5 ps) at ~10^{9} photons·pulse^{-1}·cm^{-2} was used as a source of excitation for TRPL measurement. PL decay curves were fitted by iterative re-convolution with the measured system response function. Mean photogenerated carrier lifetimes for the bi-exponential fit were calculated by the weighted average method.[38]

J-V curves were recorded in air under 100 mW/cm^{2}AM1.5G solar irradiation (PV Measurements Inc.) with a Keithley 2400 Source Meter. The light intensity for *J-V* measurements was calibrated by a standard Si solar cell and our perovskite solar cells certified by Newport.[16] External quantum efficiency (EQE) spectra were measured on a QE system (PV Measurements Inc., model IVQE8-C QE system without bias voltage)using 100 Hz chopped monochromatic light. The steady-state efficiencies were obtained by tracking the maximum output power point. The *J-V* curves for light intensity dependence were taken by neutral density filters between 1 and 100 mW/cm^{2}. The un-encapsulated cells for stability test were stored in ambient air (45% humidity and room temperature). All characterizations and measurements were performed in the ambient air.

3. Results and discussion

3.1. TRUX-E-T synthesis and characterization

The synthesis of TRUX-E-T is displayed in **Scheme 1**. A one-step Still coupling of 2,7,12-tribromo-5,5,10,10,15,15-hexahexyl-10,15-dihydro-5*H*-diindeno[1,2-*a*:1',2'-*c*]fluorene and

View Article Online
DOI: 10.1039/C7TA08053K

4-methoxy-*N*-(4-methoxyphenyl)-*N*-(4-(7-(tributylstannyl)-2,3-dihydrothieno[3,4-*b*][1,4]dioxin-5-yl)phenyl)aniline was readily afforded TRUX-E-T with a yield of 67.5%. The tribromotuxene **3** was prepared via a three-step procedure, i.e., cyclization of truxene using 1-indanone, alkylation and bromination. The tin reagent was prepared according to the literature.[43] The synthetic pathways and experimental details are available in **Electronic Supplementary Information (ESI)**. TRUX-E-T was acquired as a light-yellow solid after silica-gel column chromatography and recrystallization from methanol. During the purification of TRUX-E-T, no expensive sublimation step is involved, which is necessary for spiro-OMeTAD instead.[44] The structure of TRUX-E-T is confirmed by ^{1}H and ^{13}C NMR spectra and MALDI-TOF mass spectrometry (**Figure S1-S6**).

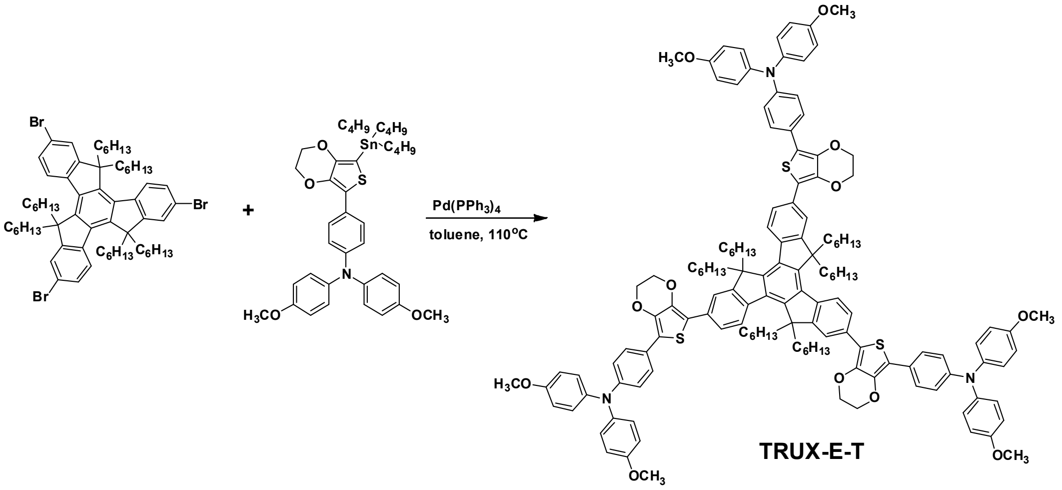

Scheme 1. Synthetic route of TRUX-E-T

Figure S7 shows thermogravimetric analysis (TGA) of TRUX-E-T, exhibiting decomposition temperature (5% weight loss) at 421°C in nitrogen atmosphere. This result indicates the excellent inherent thermal stability of TRUX-E-T, which would benefit the long-term stability of PVSCs with TRUX-E-T HSLs. Differential scanning calorimetry (DSC) shown in **Figure S8** exhibits a clear glass transition at around 202°C, indicating the amorphous nature of as-synthesized TRUX-E-T.

View Article Online
DOI: 10.1039/C7TA08053K

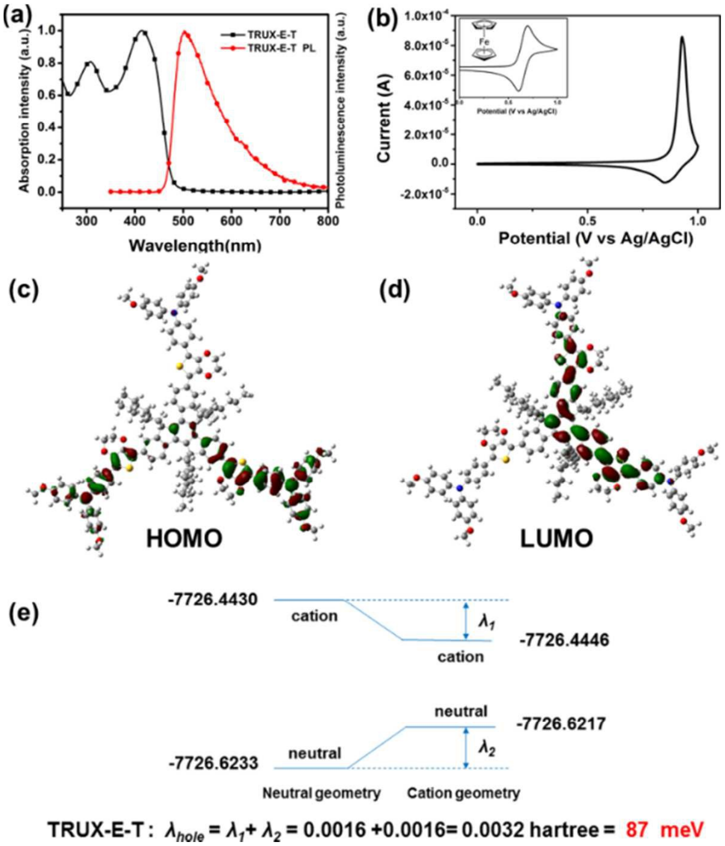

Figure 1. (a) Absorption and PL spectra of a TRUX-E-T film. (b) Cyclic voltammetry (CV) of TRUX-E-T. The inset shows CV plot for ferrocene/ferrocenium as reference. DFT-calculated electronic structure of TRUX-E-T, showing the electronic energy levels of (c) HOMO and (d) LUMO. (e) Calculation of the hole reorganization energy for TRUX-E-T.

The normalized absorption and photoluminescence (PL) spectra of a TRUX-E-T film are shown in **Figure 1a**. TRUX-E-T shows absorption of photons with an edge of 477 nm and a maximum peak located at 415 nm. The shoulder in UV region can be attributed to π-π* transition.[26] The optical bandgap (E_g^{opt}) of TRUX-E-T is estimated at 2.60 eV. PL spectrum shows that TRUX-E-T has a main emission wavelength centred at 502 nm.

To check energy levels of TRUX-E-T, electrochemical cyclic voltammetry (CV) was employed to evaluate its electrochemical properties. Ferrocene/ferrocenium was used as a reference with a potential of 0.55V vs. Ag/AgCl electrode. As shown in **Figure 1b**, a clear oxidation peak was observed. From the onset potential for oxidation (E_{ox}), the HOMO energy level was determined to be -5.10 eV for TRUX-E-T, which is favourable for hole transfer. The corresponding LUMO energy level was estimated to be -2.50 eV according to the measured E_g^{opt}.

View Article Online
DOI: 10.1039/C7TA08053K

The electronic structure and geometry of TRUX-E-T were also investigated with density functional theory (DFT) calculation using Gaussian program at the B3LYP/6-31G (d,p) level, as shown in **Figure 1c** and **d**. The dihedral angles between three arms and central truxene core are17^{o}, 21^{o}, and 22^{o}, respectively. The relatively planar molecular configuration can facilitate intermolecular interaction, and thus enhance charge transport. As shown in **Figure 1e**, the calculated hole reorganization energies (λ_{hole}) of TRUX-E-T (87meV) is much smaller than that of spiro-OMeTAD (148 meV), indicating a better hole-transporting property. We compared the hole mobility of TRUX-E-T and spiro-OMeTAD by making hole-only devices with a structure of ITO/poly(3,4-ethylenedioxythiophene):polystyrene sulfonate (PEDOT:PSS)/TRUX-E-T or spiro-OMeTAD/MoO_3/Ag. The calculation was done by space charge-limited current (SCLC) model. The hole mobilities are estimated to be 1.41×10^{-4} cm$^{2}\cdot$V$^{-1}\cdot$s^{-1} and 2.47×10^{-4} cm$^{2}\cdot$V$^{-1}\cdot$s^{-1} for spiro-OMeTAD and TRUX-E-T, respectively, as shown in **Figure S9 (Electronic Supplementary Information (ESI))**. A higher hole mobility indicates a better hole transport, benefiting the improvement in charge transport balance within PVSCs. Our calculation and experimental characterization thus reveal that TRUX-E-T is suitable as a HSL material for PVSC fabrication.

3.2. PVSC fabrication and characterization

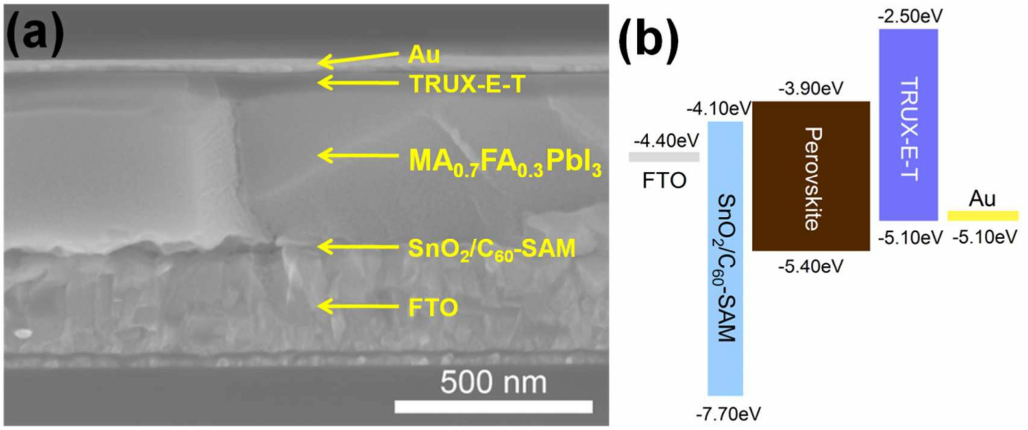

Figure 2. (a) Cross-sectional SEM image of our regular PVSC with TRUX-E-T HSL. (b) Energy band diagram of our regular PVSC with TRUX-E-T as HSL.

View Article Online
DOI: 10.1039/C7TA08053K

Figure 2a shows a cross-sectional SEM image of our PVSC using TRUX-E-T as HSL. The perovskite absorber is $MA_{0.7}FA_{0.3}PbI_3$ and the PVSC has the regular n-i-p configuration of FTO/SnO_2/C_{60}-SAM/peroskite/TRUX-E-T/Au. The SnO_2 layer was prepared by plasma-enhanced atomic-layer deposition (PEALD) and has a thickness of about 20 nm.[34, 37, 38, 40, 42]The perovskite layer was grown by a one-step deposition method and has a thickenss of about 450 nm. We find that TRUX-E-Tcan be smoothly deposited onto the perovskite absorber layer by solution processing, as evidenced by the AFM images shown in **Figure S10**. The root mean square (RMS) roughness of perovskite layer is 10.9 nm, which is reduced to 2.9 nm after the deposition of 50 nm TRUX-E-T. **Figure 2b** shows the energy level diagram of our device using TRUX-E-T HSL, presenting selective transfer of photogenerated electrons and holes, i.e., electrons are reflected by TRUX-E-T and transfer through SnO_2 and holes are reflected by SnO_2 and transfer through TRUX-E-T, which is suitable for PVSCs.

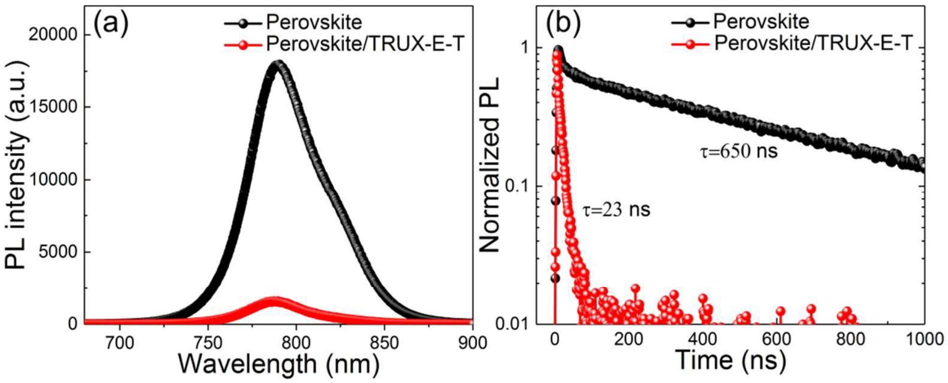

Figure 3. (a) PL spectra and (b) TRPL decays of perovskite film and perovskite/TRUX-E-T.

To evaluate the effectiveness of hole transfer at the perovskite/TRUX-E-T interface, we performed steady-state photoluminescence (PL) and time-resolved PL (TRPL) measurements on perovskite films deposited on bare glass substrates and coated with poly(methyl methacrylate) (PMMA) for protection and TRUX-E-T. As shown in **Figure 3a**, the PL emission of the perovskite film with TRUX-E-T coated shows a significant quenching as compared to that of the perovskite film with PMMA coated, indicating an effective charge transfer at the perovskite/TRUX-E-T interface. The results are consistent with the TRPL decays measured from these samples (**Figure 3b**). The deposition of TRUX-E-T layer on perovskite shortens the mean carrier lifetime for perovskite from 650 ns to 23 ns, confirming

View Article Online
DOI: 10.1039/C7TA08053K

a fast charge transfer at the perovskite/TRUX-E-T interface.

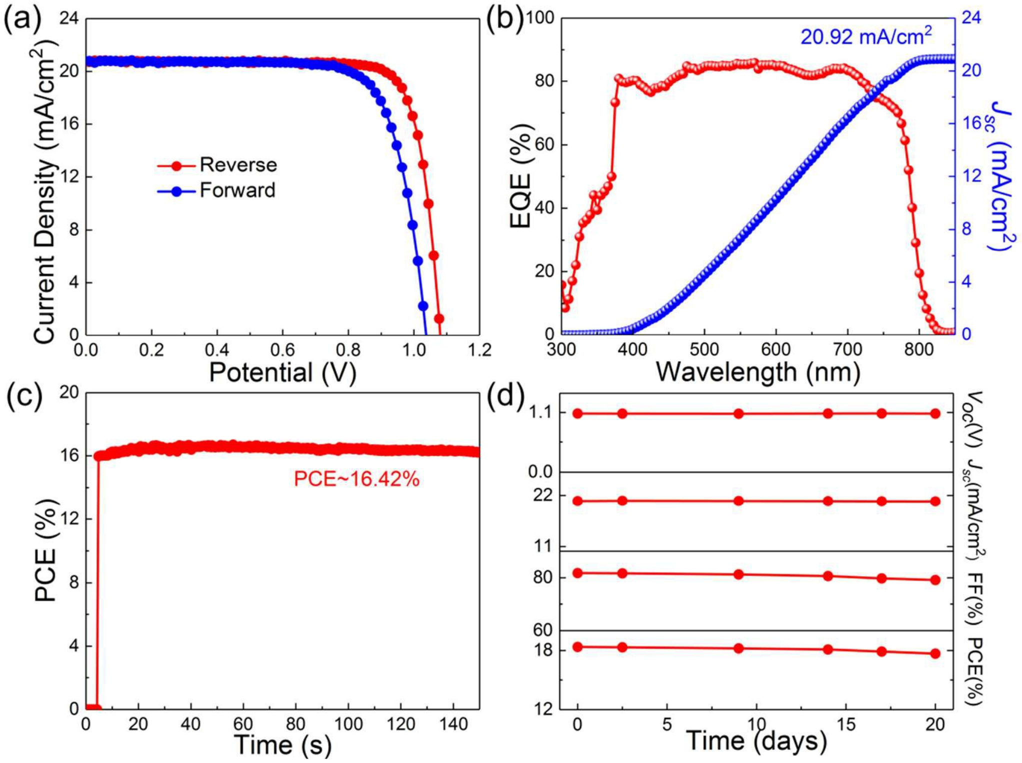

Figure 4. (a) *J-V* curves of our best-performing PVSC with TRUX-E-T HSL measured under AM 1.5G illumination at reverse and forward voltage scans. (b) EQE spectrum and integrated J_{sc} of the best-performing PVSC based on TRUX-E-T HSL. (c) Maximum power point tracking of PCE and (d) Photovoltaic parameters versus time of PVSC with TRUX-E-T HSL.

Figure 4a shows the current density-voltage (*J-V*) curves of the best-performing PVSC using a 50 nm TRUX-E-T HSL measured under reverse and forward voltage scans.Our champion cell achieves a PCE of 18.36 (16.44)% with a V_{oc} of 1.08 (1.04) V, a J_{sc} of 20.8 (20.8) mA/cm^2, and a FF of 81.8 (76.2)% when measured under reverse (forward) voltage scan. This performance is slightly lower than that of the PVSC with spiro-OMeTAD HSLs (PCE of 19.13 (18.12)% with a V_{oc} of 1.10 (1.09) V, a J_{sc} of 21.9 (21.9) mA/cm^2, and a FF of 78.7 (76.4)% under reverse (forward) voltage scan), as shown in **Figure S11**. Since the *J-V* hysteresis has been found in both PVSCs with TRUX-E-T and spiro-OMeTAD HSLs, it might be attributed to the ESL/perovskite interface[37, 40] or perovskite film itself such as ion migration,[45] and/or trap states.[46] The EQE spectrum of this cell is shown in **Figure 4b**. The integrated J_{sc} of over a 100 mW/cm^2 AM1.5G solar spectrumis 20.92 mA/cm^2, which is in good agreement with the J_{sc} obtained from the *J-V* curves. The stabilized PCE measured by

View Article Online
DOI: 10.1039/C7TA08053K

the tracking maximum power point is 16.42% (**Figure 4c**). As mentioned above, TRUX-E-T has a good thermal stability, which can help to improve the stability of PVSCs. Therefore, we measured the dependence of each photovoltaic parameter of un-encapsulated PVSCs with TRUX-E-T HSLs stored in dark and glove box on the storage time. As shown in **Figure 4d**, the cell exhibited a good stability for 20 days, maintaining 96.4% of its initial efficiency of 18.35% when measued under reserse voltage scan and in ambient. The main degradation originates from FFs dropping from 81.8% to 79.2%, which is likely attributed to the contact damage of our measured cell with isolated pixel. In other words, the results suggest an encouragingalternative HSL for stable PVSCs.

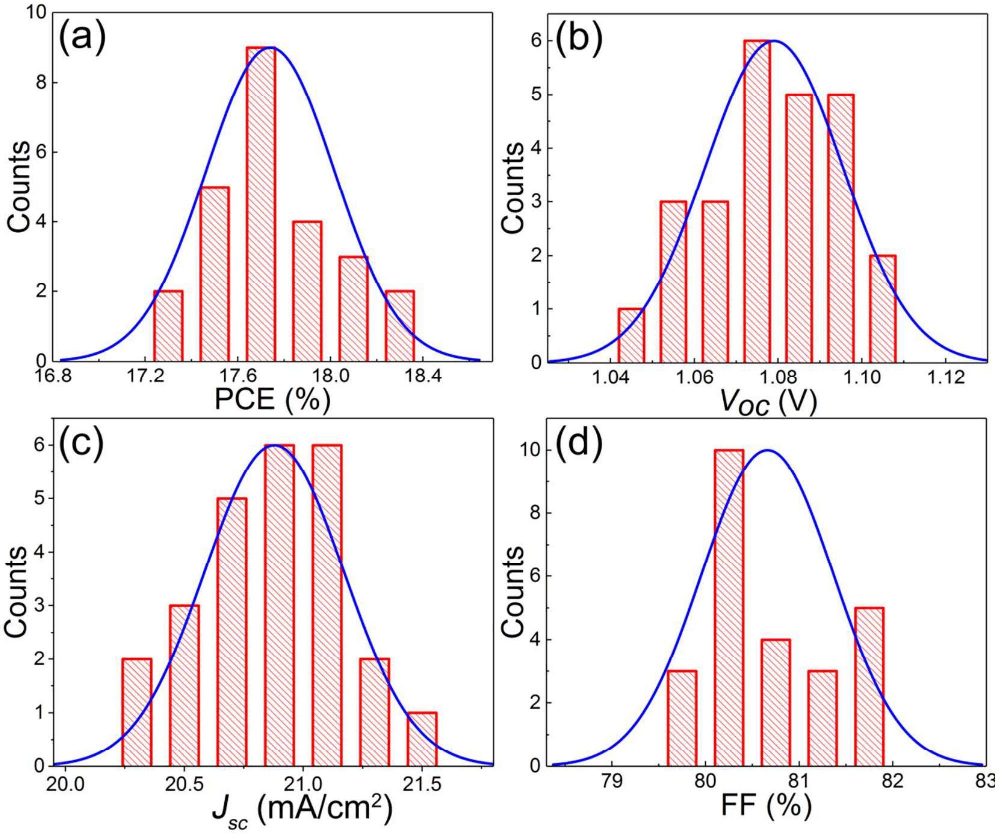

Figure 5. Histograms of (a) PCEs, (b) FFs, (c) V_{oc}s, and (d) J_{sc}s measured for 25 cells with TRUX-E-T-based PVSCs.

To evaluate the performance reproducibility of PVSCs using the TRUX-E-T HSLs, we fabricated and measured 25 PVSCs. The histograms of the PCE, V_{oc}, J_{sc}, and FF measured under reverse voltage scan are shown in **Figure 5a, b, c, and d**, respectively. The average PCE, V_{oc}, J_{sc}, and FF for these 25 cells are 17.74±0.62%, 1.08±0.03V, 20.88±0.65 mA/cm^2,

View Article Online
DOI: 10.1039/C7TA08053K

and 80.7±1.2%, respectively, revealing a good reproducibility.

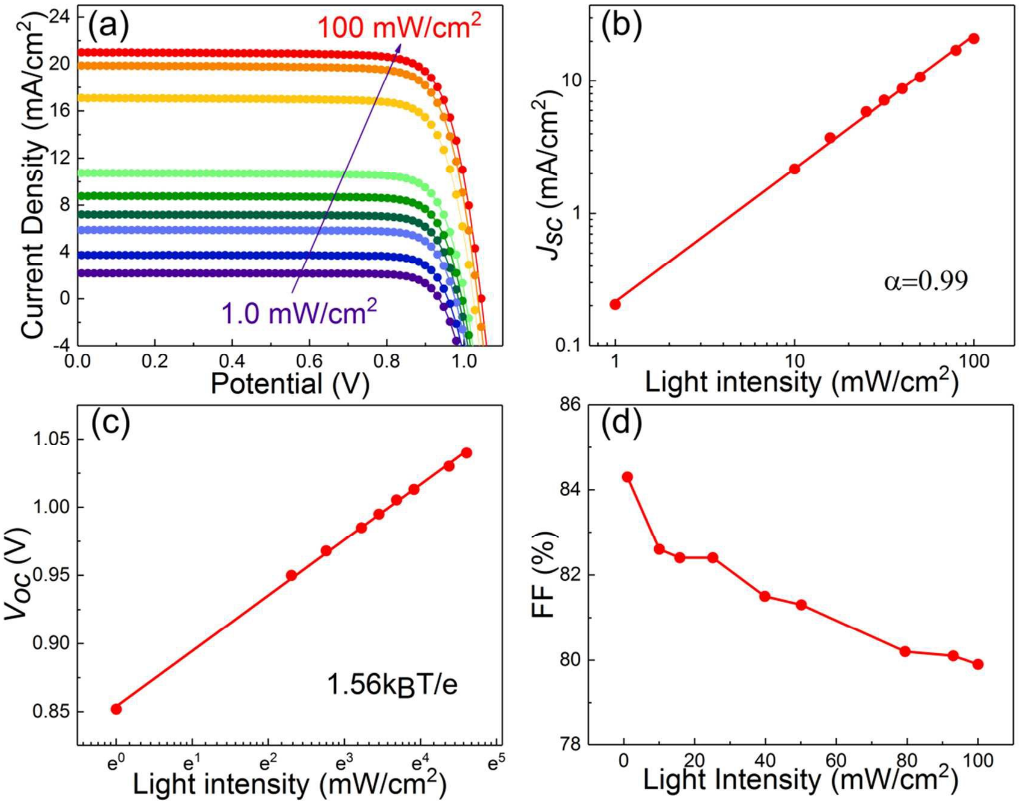

Figure 6. (a) *J-V* curves of a PVSC with TRUX-E-T HSLs under different light intensities ranging from 1 to 100 mW/cm^2. Light intensity dependence: (b) J_{sc} versus light intensity; (c) V_{oc} versus light intensity; (d) FF versus light intensity.

To understand the charge extraction and recombination mechanism in the PVSCs with TRUX-E-T HSLs, the *J-V* characteristics were measured under light intensities varying from 1 to 100 mW/cm^2, as shown in **Figure 6a**. **Figure 6b** shows the power law relationship between J_{sc} and light intensity. It is known that a carrier imbalance or an interfacial barrier could lead to a space charge limited solar cell with α ~ 0.75.[47-49] An α value close to 1 means a solar cell with no space charge effect.[47-49] The PVSC with TRUX-E-T HSL does not appear to be space charge limited since the α is 0.99, indicating an efficient charge transfer in this solar cell. The natural logarithmic relationship between light intensity and V_{oc} has a slope of 1.56k$_B$T/q, as shown in **Figure 6c**, implying that Shockley Reed Hall recombination is dominant in solar cells,[50-52] which is also consistent with the fact that the FF decreases when the light intensity increases from 1 to 100 mW/cm^2 (**Figure 6d**). Therefore, the high FF originates from the efficient charge transfer at the perovskite/HSL interface due to the appropriate HOMO level and high hole mobility of HSLs.

The estimated lab synthesis and purification cost of TRUX-E-T is about $38.9/g (see cost calculation for TRUX-E-T in **Electronic Supplementary Information (ESI)**), which is one thirteenth of that of spiro-OMeTAD (about $500/g).[53] Furthermore, the typical thickness of spiro-OMeTAD for efficient PVSCs is around 150 nm, while the thickness of TRUX-E-T HSLs used in our PVSCs is only about 50 nm. Therefore, the unit cost of TRUX-E-T used in PVSCs is roughly one 40th of that of spiro-OMeTAD.[53] Therefore, our TRUX-E-T HSL offers an attractive potential to commercialization of the emerging PVSC technology.

4. Conclusions

We have synthesized and characterized TRUX-E-T, a new small molecule-based HSL material using a facile route. Characterizations reveal that TRUX-E-T is suitable as HSL for PVSCs. We found that TRUX-E-T can be smoothly deposited on perovskite layers, enabling PVSC to use thin TRUX-E-T layers. Our best-performing PVSCs use only ~50nm thick TRUX-E-THSLs, which facilitates the reduction in device cost. The estimated unit cost of TRUX-E-T used in PVSCs is roughly one 40th of that of spiro-OMeTAD. Finally, TRUX-E-T exhibits hole mobility as high as 2.47×10^{-4} cm^2/Vs, which is responsible for the high FFs of up to 82% obtained in our PVSCs using thin TRUX-E-THSLs.

Acknowledgements

This work was supported by the National Natural Science Foundation of China (51671148, 51271134, J1210061, 11674251, 51501132, 51601132), the Hubei Provincial Natural Science Foundation of China (2016CFB446, 2016CFB155), the Fundamental Research Funds for the Central Universities, and the CERS-1-26 (CERS-China Equipment and Education Resources System), and the China Postdoctoral Science Foundation (2014T70734), and the Open Research Fund of Science and Technology on High Strength Structural Materials Laboratory (Central South University) and the Suzhou Science and Technology project (No. SYG201619). The design of TRUX-E-T was completed by the W. Tang’s group at Nanjing

View Article Online
DOI: 10.1039/C7TA08053K

University of Science and Technology under the financial support from the National Natural Science Foundation of China (Grant No. 51573077), the Jiangsu Province Natural Science Foundation for Distinguished Young Scholars (BK20130032), the Program for New Century Excellent Talents in University (NCET-12-0633), and the Priority Academic Program Development of Jiangsu Higher Education Institutions. This work was also financially supported by the U.S. Department of Energy (DOE) SunShot Initiative under the Next Generation Photovoltaics 3 program (DE-FOA-0000990), National Science Foundation under contract no. CHE−1230246 and DMR−1534686, and the Ohio Research Scholar Program. Ellingson's group at the University of Toledo received financial support from the National Science Foundation under contract no. CHE−1230246, and from University of Toledo startup funds.

References

1. Q. Dong, Y. Fang, Y. Shao, P. Mulligan, J. Qiu, L. Cao and J. Huang, *Science*, 2015, **347**, 967-970.
2. D. B. Mitzi, S. Wang, C. A. Feild, C. A. Chess and A. M. Guloy, *Science*, 1995, **267**, 1473-1476.
3. B. Saparov and D. B. Mitzi, *Chem. Rev.*, 2016, **116**, 4558-4596.
4. W.-J. Yin, T. Shi and Y. Yan, *Adv. Mater.*, 2014, **26**, 4653-4658.
5. S. D. Stranks, G. E. Eperon, G. Grancini, C. Menelaou, M. J. P. Alcocer, T. Leijtens, L. M. Herz, A. Petrozza and H. J. Snaith, *Science*, 2013, **342**, 341-344.
6. G. Xing, N. Mathews, S. Sun, S. S. Lim, Y. M. Lam, M. Grätzel, S. Mhaisalkar and T. C. Sum, *Science*, 2013, **342**, 344-347.
7. W. S. Yang, B.-W. Park, E. H. Jung, N. J. Jeon, Y. C. Kim, D. U. Lee, S. S. Shin, J. Seo, E. K. Kim, J. H. Noh and S. I. Seok, *Science*, 2017, **356**, 1376-1379.
8. M. Liu, M. B. Johnston and H. J. Snaith, *Nature*, 2013, **501**, 395-398.
9. H. Zhou, Q. Chen, G. Li, S. Luo, T.-b. Song, H.-S. Duan, Z. Hong, J. You, Y. Liu and Y. Yang, *Science*, 2014, **345**, 542-546.
10. A. Kojima, K. Teshima, Y. Shirai and T. Miyasaka, *J. Am. Chem. Soc.*, 2009, **131**, 6050-6051.
11. H.-S. Kim, C.-R. Lee, J.-H. Im, K.-B. Lee, T. Moehl, A. Marchioro, S.-J. Moon, R. Humphry-Baker, J.-H. Yum, J. E. Moser, M. Gratzel and N.-G. Park, *Sci. Rep.*, 2012, **2**, 591.
12. N. Ahn, D.-Y. Son, I.-H. Jang, S. M. Kang, M. Choi and N.-G. Park, *J. Am. Chem. Soc.*, 2015, **137**, 8696-8699.
13. W. Ke, G. Fang, Q. Liu, L. Xiong, P. Qin, H. Tao, J. Wang, H. Lei, B. Li, J. Wan, G. Yang and Y. Yan, *J. Am. Chem. Soc.*, 2015, **137**, 6730-6733.
14. D. Bi, C. Yi, J. Luo, J.-D. Décoppet, F. Zhang, Shaik M. Zakeeruddin, X. Li, A. Hagfeldt and M. Grätzel, *Nat. Energy*, 2016, **1**, 16142.
15. M. Yang, Z. Li, M. O. Reese, O. G. Reid, D. H. Kim, S. Siol, T. R. Klein, Y. Yan, J. J. Berry, M. F. A. M. van Hest and K. Zhu, *Nat. Energy*, 2017, **2**, 17038.

View Article Online
DOI: 10.1039/C7TA08053K

16. D. Zhao, Y. Yu, C. Wang, W. Liao, N. Shrestha, C. R. Grice, A. J. Cimaroli, L. Guan, R. J. Ellingson, K. Zhu, X. Zhao, R.-G. Xiong and Y. Yan, *Nat. Energy*, 2017, **2**, 17018.
17. Y. Shao, Y. Yuan and J. Huang, *Nat. Energy*, 2016, **1**, 15001.
18. D. Zhao, M. Sexton, H.-Y. Park, G. Baure, J. C. Nino and F. So, *Adv. Energy Mater.*, 2015, **5**, 1401855.
19. A. Krishna and A. C. Grimsdale, *J. Mater. Chem. A*, 2017, **5**, 16446-16466.
20. J. Burschka, A. Dualeh, F. Kessler, E. Baranoff, N.-L. Cevey-Ha, C. Yi, M. K. Nazeeruddin and M. Grätzel, *J. Am. Chem. Soc.*, 2011, **133**, 18042-18045.
21. L. Calió, S. Kazim, M. Grätzel and S. Ahmad, *Angew. Chem. Int. Ed.*, 2016, **55**, 14522-14545.
22. J.-P. Correa-Baena, A. Abate, M. Saliba, W. Tress, T. Jesper Jacobsson, M. Gratzel and A. Hagfeldt, *Energy Environ. Sci.*, 2017, **10**, 710-727.
23. W. Yan, S. Ye, Y. Li, W. Sun, H. Rao, Z. Liu, Z. Bian and C. Huang, *Adv. Energy Mater.*, 2016, DOI: 10.1002/aenm.201600474.
24. X. Yin, Q. An, J. Yu, F. Guo, Y. Geng, L. Bian, Z. Xu, B. Zhou, L. Xie, F. Zhang and W. Tang, 2016, **6**, 25355.
25. K. Rakstys, A. Abate, M. I. Dar, P. Gao, V. Jankauskas, G. Jacopin, E. Kamarauskas, S. Kazim, S. Ahmad, M. Grätzel and M. K. Nazeeruddin, *J. Am. Chem. Soc.*, 2015, **137**, 16172-16178.
26. K. Rakstys, S. Paek, P. Gao, P. Gratia, T. Marszalek, G. Grancini, K. T. Cho, K. Genevicius, V. Jankauskas, W. Pisula and M. K. Nazeeruddin, *J. Mater. Chem. A*, 2017, **5**, 7811-7815.
27. C. Huang, W. Fu, C.-Z. Li, Z. Zhang, W. Qiu, M. Shi, P. Heremans, A. K. Y. Jen and H. Chen, *J. Am. Chem. Soc.*, 2016, **138**, 2528-2531.
28. J.-L. Wang, Z.-M. Tang, Q. Xiao, Y. Ma and J. Pei, *Org. Lett.*, 2009, **11**, 863-866.
29. P.-Y. Su, L.-B. Huang, J.-M. Liu, Y.-F. Chen, L.-M. Xiao, D.-B. Kuang, M. Mayor and C.-Y. Su, *J. Mater. Chem. A*, 2017, **5**, 1913-1918.
30. P. Ganesan, K. Fu, P. Gao, I. Raabe, K. Schenk, R. Scopelliti, J. Luo, L. H. Wong, M. Gratzel and M. K. Nazeeruddin, *Energy Environ. Sci.*, 2015, **8**, 1986-1991.
31. H. Li, K. Fu, A. Hagfeldt, M. Grätzel, S. G. Mhaisalkar and A. C. Grimsdale, *Angew. Chem. Int. Ed.*, 2014, **53**, 4085-4088.
32. J. Wang, K. Liu, L. Ma and X. Zhan, *Chem. Rev.*, 2016, **116**, 14675-14725.
33. H. Chen, W. Fu, C. Huang, Z. Zhang, S. Li, F. Ding, M. Shi, C.-Z. Li, A. K. Y. Jen and H. Chen, *Adv. Energy Mater.*, 2017, DOI: 10.1002/aenm.201700012, 1700012.
34. Y. Yu, C. Wang, C. R. Grice, N. Shrestha, J. Chen, D. Zhao, W. Liao, A. J. Cimaroli, P. J. Roland, R. J. Ellingson and Y. Yan, *ChemSusChem*, 2016, **9**, 3288-3297.
35. M. L. Petrus, T. Bein, T. J. Dingemans and P. Docampo, *J. Mater. Chem. A*, 2015, **3**, 12159-12162.
36. W. Ke, C. Xiao, C. Wang, B. Saparov, H.-S. Duan, D. Zhao, Z. Xiao, P. Schulz, S. P. Harvey, W. Liao, W. Meng, Y. Yu, A. J. Cimaroli, C.-S. Jiang, K. Zhu, M. Al-Jassim, G. Fang, D. B. Mitzi and Y. Yan, *Adv. Mater.*, 2016, **28**, 5214-5221.
37. C. Wang, C. Xiao, Y. Yu, D. Zhao, R. A. Awni, C. R. Grice, K. Ghimire, D. Constantinou, W. Liao, A. J. Cimaroli, P. Liu, J. Chen, N. J. Podraza, C.-S. Jiang, M. M. Al-Jassim, X. Zhao and Y. Yan, *Adv. Energy Mater.*, 2017, DOI: 10.1002/aenm.201700414, DOI: 10.1002/aenm.201700414.
38. C. Wang, D. Zhao, C. R. Grice, W. Liao, Y. Yu, A. Cimaroli, N. Shrestha, P. J. Roland, J. Chen, Z. Yu, P. Liu, N. Cheng, R. J. Ellingson, X. Zhao and Y. Yan, *J. Mater. Chem. A*, 2016, **4**,

View Article Online
DOI: 10.1039/C7TA08053K

12080-12087.
39. C. Wang, L. Guan, D. Zhao, Y. Yu, C. R. Grice, Z. Song, R. A. Awni, J. Chen, J. Wang, X. Zhao and Y. Yan, *ACS Energy Lett.*, 2017, DOI: 10.1021/acsenergylett.7b00644, 2118-2124.
40. C. Wang, D. Zhao, Y. Yu, N. Shrestha, C. R. Grice, W. Liao, A. J. Cimaroli, J. Chen, R. J. Ellingson, X. Zhao and Y. Yan, *Nano Energy*, 2017, **35**, 223-232.
41. X. Yin, L. Guan, J. Yu, D. Zhao, C. Wang, N. Shrestha, Y. Han, Q. An, J. Zhou, B. Zhou, Y. Yu, C. R. Grice, R. A. Awni, F. Zhang, J. Wang, R. J. Ellingson, Y. Yan and W. Tang, *Nano Energy*, 2017, **40**, 163-169.
42. Y. Yu, C. Wang, C. R. Grice, N. Shrestha, D. Zhao, W. Liao, L. Guan, R. A. Awni, W. Meng, A. J. Cimaroli, K. Zhu, R. J. Ellingson and Y. Yan, *ACS Energy Lett.*, 2017, DOI: 10.1021/acsenergylett.7b00278, 1177-1182.
43. Q. Feng, X. Jia, G. Zhou and Z.-S. Wang, *Chem. Commun.*, 2013, **49**, 7445-7447.
44. W. Liao, D. Zhao, Y. Yu, N. Shrestha, K. Ghimire, C. R. Grice, C. Wang, Y. Xiao, A. J. Cimaroli, R. J. Ellingson, N. J. Podraza, K. Zhu, R.-G. Xiong and Y. Yan, *J. Am. Chem. Soc.*, 2016, **138**, 12360-12363.
45. B. Chen, M. Yang, X. Zheng, C. Wu, W. Li, Y. Yan, J. Bisquert, G. Garcia-Belmonte, K. Zhu and S. Priya, *The Journal of Physical Chemistry Letters*, 2015, DOI: 10.1021/acs.jpclett.5b02229, 4693-4700.
46. Y. Shao, Z. Xiao, C. Bi, Y. Yuan and J. Huang, *Nat. Commun.*, 2014, **5**, 5784.
47. D. Bi, L. Yang, G. Boschloo, A. Hagfeldt and E. M. J. Johansson, *J. Phys. Chem. Lett.*, 2013, **4**, 1532-1536.
48. L. J. A. Koster, V. D. Mihailetchi, H. Xie and P. W. M. Blom, *Appl. Phys. Lett.*, 2005, **87**, 203502.
49. V. D. Mihailetchi, J. Wildeman and P. W. M. Blom, *Phys. Rev. Lett.*, 2005, **94**, 126602.
50. S. R. Cowan, W. L. Leong, N. Banerji, G. Dennler and A. J. Heeger, *Adv. Funct. Mater.*, 2011, **21**, 3083-3092.
51. R. N. Hall, *Phys. Rev.*, 1952, **87**, 387-387.
52. W. Shockley and W. T. Read, *Phys. Rev.*, 1952, **87**, 835-842.
53. M. Saliba, S. Orlandi, T. Matsui, S. Aghazada, M. Cavazzini, J.-P. Correa-Baena, P. Gao, R. Scopelliti, E. Mosconi, K.-H. Dahmen, F. De Angelis, A. Abate, A. Hagfeldt, G. Pozzi, M. Graetzel and M. K. Nazeeruddin, *Nat. Energy*, 2016, **1**, 15017.

View Article Online
DOI: 10.1039/C7TA08053K

Table of contents entry

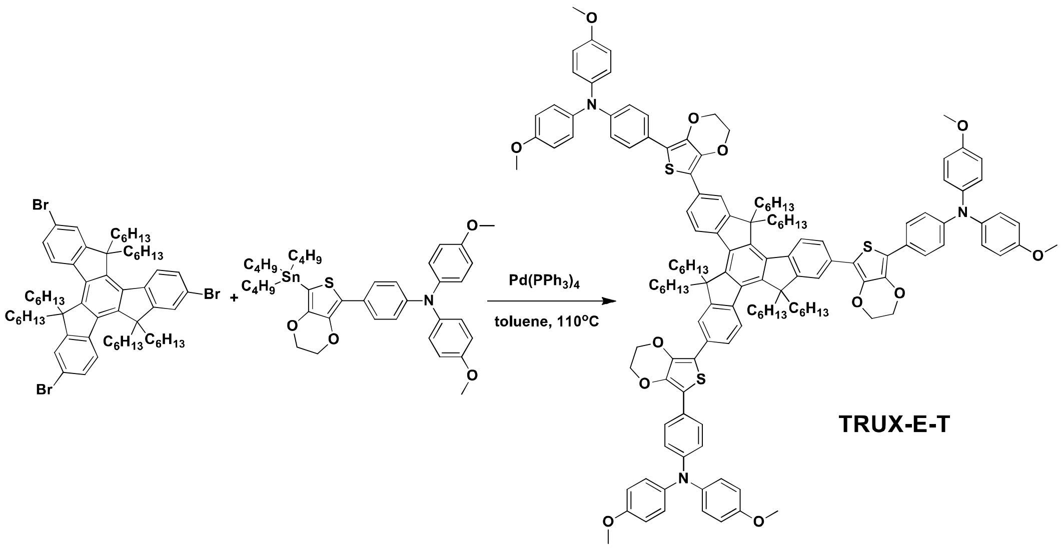

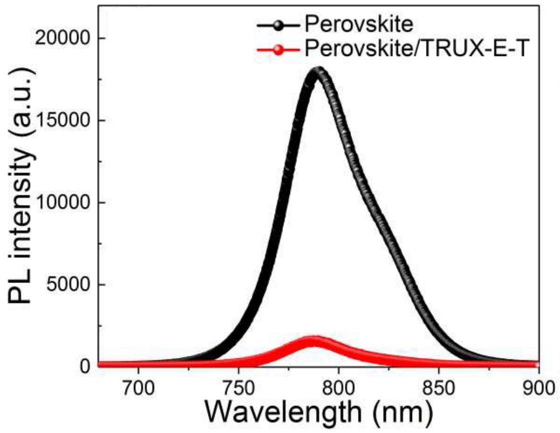

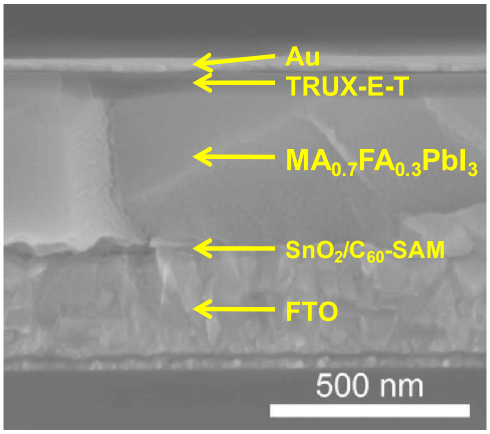

A cost-effective truxene-based hole selective material has been synthesized by facile approach, leading to efficient perovskite solar cells with 82% FFs.